Molecular random tilings as glasses

Juan P. Garrahan[1], Andrew Stannard, Matthew O. Blunt, and Peter H. Beton

School of Physics and Astronomy, University of Nottingham, Nottingham NG7 2RD, United Kingdom

Edited by Hans C. Andersen, Stanford University, Stanford, CA, and approved July 17, 2009 (received for review March 9, 2009)

We have recently shown that *p*-terphenyl-3,5,3′,5′-tetracarboxylic acid adsorbed on graphite self-assembles into a two-dimensional rhombus random tiling. This tiling is close to ideal, displaying long-range correlations punctuated by sparse localized tiling defects. In this article we explore the analogy between dynamic arrest in this type of random tilings and that of structural glasses. We show that the structural relaxation of these systems is via the propagation–reaction of tiling defects, giving rise to dynamic heterogeneity. We study the scaling properties of the dynamics and discuss connections with kinetically constrained models of glasses.

dimer coverings | dynamic heterogeneity | glass transition | lozenge tilings

Dimer coverings of lattices and random polygon tilings are problems of great interest both in physics and mathematics (1–5). One of the reasons is that they correspond to the idealized description of systems that display entropically stabilized critical phases and fractional excitations, being therefore relevant to condensed-matter systems such as quasicrystals (6, 7) and frustrated antiferromagnets (8–10).

However, actual experimental realizations of dimer covering/random tiling systems are very rare. Fig. 1 shows one of them: a molecular network formed by organic molecules adsorbed from solution onto a graphite substrate (11). The molecule *p*-terphenyl-3,5,3′,5′-tetracarboxylic acid (TPTC) (see Fig. 1*A*) binds to other TPTC molecules on the substrate adopting one of three possible orientations. Each molecule can then be mapped to a rhombus tile (see Fig. 1*B*), where the colors red, green, and blue indicate the molecular orientation. Neighboring molecules (tiles) can bind to neighbors in a parallel or "arrowhead" configuration, equivalent to junctions between tiles of the same or different color, respectively. Fig. 1*C* shows a scanning tunneling microscope (STM) image of the resulting molecular network of adsorbed TPTC, and Fig. 1*D* shows the corresponding rhombus tiling (11), where each molecule is represented by a tile.

The molecular networks studied in ref. 11 are close to "perfect" rhombus tilings (or dimer coverings of the honeycomb lattice) (1–3, 8) in the sense that they contain rather few tiling defects, typically less than one defect per 300 adsorbed molecules (11). In Fig. 1 *C* and *D*, one such tiling defect is identified. They are also entropically stabilized "random tilings" displaying algebraic spatial correlations (11), characteristic of a critical, or Coulomb, phase (1–3, 8). The structures, such as those in Fig. 1, are close to dynamically arrested at room temperature (11). The interaction energy between two neighboring molecules is several times k_BT (11), so once a tiling is formed, tile removal is highly suppressed and structural relaxation is slow. Tile rearrangements mediated by propagation of defects have been observed experimentally, but so far on timescales of seconds for each event (11). This combination of an amorphous structure, albeit with critical spatial correlations, and very slow relaxation suggests an analogy between this kind of random tiling and structural glass formers (for reviews on the glass transition, see refs. 12–14).

The aim of this article is to discuss this analogy. For simplicity, we focus on the case where all tile–tile interactions are equal, because the dynamics for small bias* is qualitatively the same in the long-time dynamical regime; the initial growth dynamics will be discussed elsewhere. We show by means of numerical simulations that the low temperature dynamics of a rhombus tiling where the number of tiles is not conserved displays some of the features observed in the dynamics of structural glass formers, in particular dynamic heterogeneity. Relaxation in these random tilings is facilitated by tiling defects, a mechanism similar to that of kinetically constrained models of glasses. We will also discuss this connection.

Model

We simulate a dimer covering of the honeycomb lattice, which is equivalent to a rhombus tiling of the plane (1–3). That is, each rhombus tile is composed of an upward- and downward-pointing triangle face-to-face; these triangles are centered at the sites of a honeycomb lattice, each in a different sublattice. The dynamics we consider is one where the only possible moves are (*i*) the adsorption of a tile on the lattice if the two sites it would occupy are empty or (*ii*) the desorption of a tile. The number or tiles (and of tiling defects) is therefore not conserved. This resembles the experimental situation where molecules are exchanged between substrate and solution (11). We consider only single-tile moves.† We set the binding energy J between neighboring tiles to $J = 1$. For low temperatures, $T < 1$ (in units of J, and where $k_B = 1$), we simulate the dynamics using a version of Borz–Kalos–Lebowitz, or continuous-time, Monte Carlo (20, 21), which is particularly efficient for this problem. We simulate systems of sizes $N = 200 \times 200$ to $N = 10^3 \times 10^3$ at all temperatures.

At low temperatures, when the density of tiles is high, desorption of tiles is rare. The energy barrier to remove a tile surrounded by four neighboring tiles is $\Delta E = 4$, and the rate for that transition is suppressed by a factor of $e^{-4/T}$. A more likely transition is the removal of a tile neighboring a defect, because the rate for this process scales as $e^{-3/T}$. This will give rise to the effective propagation of tiling defects, as sketched in Fig. 1 *E–L*. In Fig. 1*E* there are two tiling defects of opposite "charge" (3). Fig. 1*F* shows the desorption of a tile next to the leftmost defect (a process of rate $\propto e^{-3/T}$) and Fig. 1*G* the subsequent adsorption of another tile [a process of rate $O(1)$, because it is energetically favorable]. The net effect is the hopping of the defect by one (sub)lattice site. The sequence represented in Fig. 1 *G–I* shows a second such step. The effective hopping rate is therefore $\Gamma \propto e^{-3/T}$.

Author contributions: J.P.G., A.S., M.O.B., and P.H.B. performed research and J.P.G. and P.H.B. wrote the paper.

The authors declare no conflict of interest.

This article is a PNAS Direct Submission.

†To whom correspondence should be addressed. E-mail: juan.garrahan@nottingham.ac.uk.

*Due to a slight mismatch in the distance between the two end phenyl rings in a TPTC molecule and that between phenyl rings across a carboxylic–carboxylic hydrogen bond, the tilings of ref. 11 are not "ideal" (3) because there is a small energetic penalty for the parallel tile arrangement. They are "interacting" random tilings (15–18). This difference in energy is however below the critical value at which such tilings would undergo a Kosterlitz–Thouless (KT) transition to an ordered phase (18).

†In particular, we ignore moves where a cluster of tiles can be replaced without disturbing neighboring tiles. For example, in Fig. 1 *E–G* there is a central cluster of three tiles, red–blue–green, forming a hexagon of side one. This triplet can be replaced by a green–red–blue combination without disturbing the surroundings. These kinds of moves are usually the ones considered for perfect tilings (see, e.g., ref. 19). In our case, they would be suppressed due to the energy cost of removing three tiles. Furthermore, we do not consider moves where tiles "slide" on the substrate, because this kind of process does not seem to apply to the experimental situation of ref. 11 either.

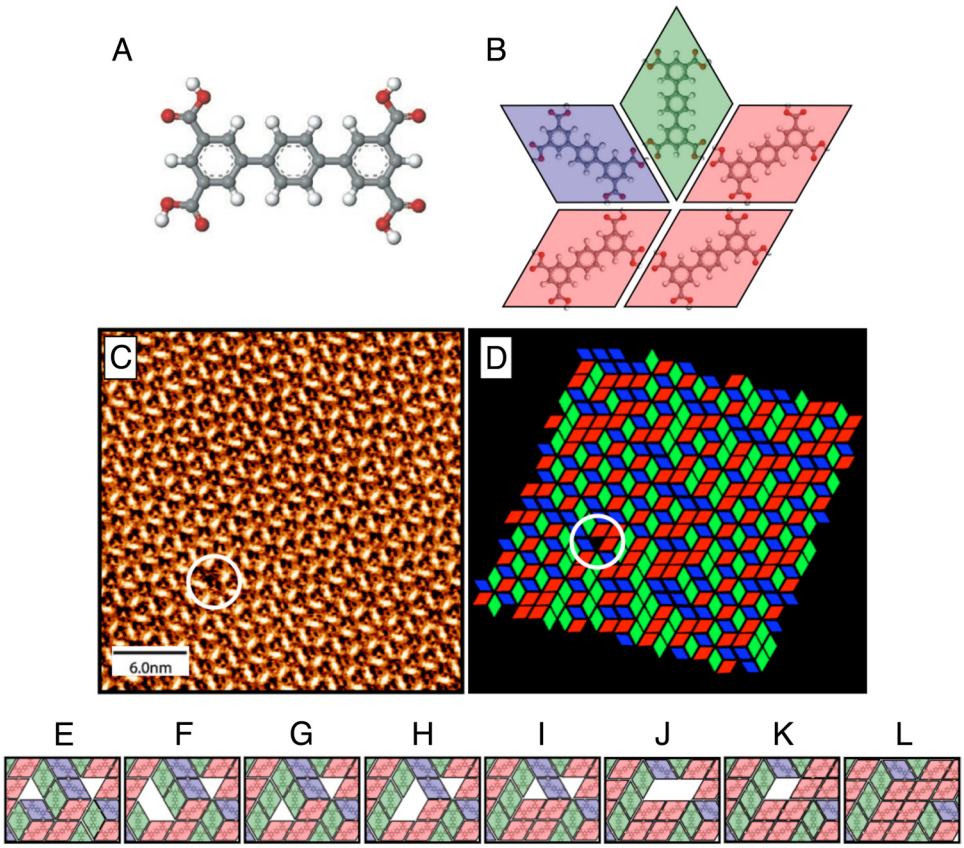

Fig. 1. Mapping of molecular network to a random rhombus tiling. (*A*) Molecular ball and stick diagram of TPTC. (*B*) Example of an arrangement of TPTC molecules linked via hydrogen bonds when adsorbed on substrate, and rhombus tile representation; the tiles are colored according to the three possible orientations of the molecule. (*C* and *D*) Mapping to a rhombus tiling. (*C*) An STM image of a typical area of TPTC network adsorbed on graphite; the backbones of the TPTC molecules appear as bright rods in the image. (*D*) The corresponding rhombus tiling. The molecular network is a rhombus tiling of the plane or, equivalently, a dimer covering of the honeycomb lattice. The white circle shows the position of a tiling defect. (*E*–*L*) Example of motion of tiling defects: The leftmost defect (upward pointing triangle) effectively makes two hopping steps, between *E* and *G* and between *G* and *I*. This motion is mediated by the desorption (*F* and *H*) and readsorption (*G* and *I*) of a tile. Between *I* and *K*, the rightmost defect (downward pointing triangle) makes a step to the left, which brings it into contact with the leftmost defect. (*L*) The two annihilate with the adsorption of the last tile (see ref. 11 for details.)

Defects of opposite charge can effectively react with each other. This is sketched in Fig. 1 *I*–*L*. In this case, the rightmost defect hops one step to the left. Upon meeting the opposite defect, a gap large enough for a tile is formed, and the two defects are "annihilated" by the adsorption of a tile, at rate $O(1)$ because this is energetically favorable. Of course, this process is reversible, and two opposing defects can be "created" by desorption of a molecular tile, at a rate $\propto e^{-4/T}$. The effective dynamics of defects, therefore, resembles a reversible $A + B \rightarrow 0$ reaction–diffusion process (22); although, as we will see below, it is not clear that defect propagation is actually diffusive or that defect interaction can be approximated as being local (see also refs. 23 and 24).

Results

Fig. 2*A* shows the evolution in time of the concentration of defects, $c(t)$, starting from an empty lattice at time 0, $c(0) = 1$, at various temperatures, T. After a short initial transient of fast, temperature-independent, tile adsorption, the system enters a regime of activated dynamics: Most defects are isolated, and energy barriers need to be crossed for the dynamics to progress. The dynamics becomes increasingly sluggish with decreasing temperature, and once times are long enough for defect motion to take place relaxation enters a scaling regime. Fig. 2*B* shows that the rate-limiting step is defect hopping: The long time data collapses if time is rescaled by the defect hopping rate, $t \rightarrow \Gamma t$. The defect concentration decays as $c(t) \sim (\Gamma t)^{-\alpha}$, with $\alpha \approx 3/4$. This exponent is somewhat different from the exponent $\alpha = 1/2$ of two-species diffusion–annihilation, $A + B \rightarrow 0$, in dimension two (22, 25). This could be an indication that defect propagation is nondiffusive, although an exponent of $\alpha = 3/4$ can also be explained by initial state fluctuations in the tiling case that differ

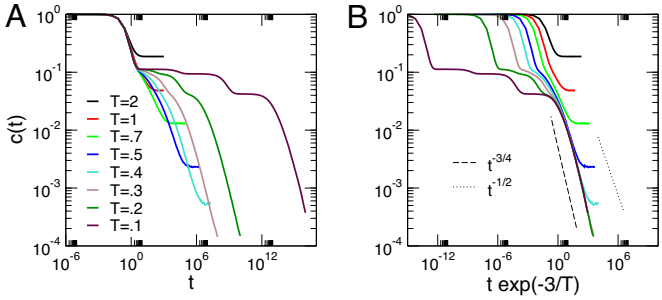

Fig. 2. Relaxation to equilibrium in the random rhombus tiling. (*A*) Relaxation of the concentration of defects $c(t)$ as a function of time (in units of Monte Carlo sweeps), starting from an empty lattice, $c(0) = 1$, for various temperatures T. (*B*) Same as *A*, but time is rescaled by the defect effective hopping rate $\Gamma \approx e^{-3/T}$. The curves collapse at long times in this representation. The dotted line indicates the power-law decay $(\Gamma t)^{-1/2}$ expected from diffusion–pair-annihilation, $A + B \rightarrow 0$, in $d = 2$. The observed behavior is closer to $c(t) \sim (\Gamma t)^{-3/4}$, as indicated by the dashed line.

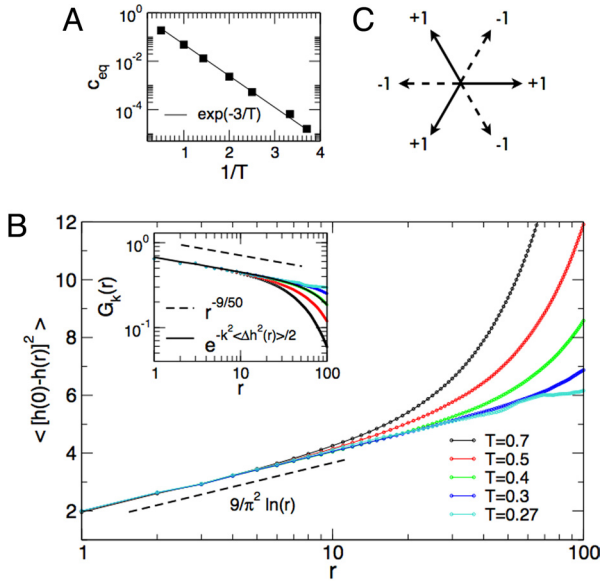

Fig. 3. Equilibrium properties of random rhombus tiling. (*A*) Equilibrium concentration of defects, c_{eq}, as a function of temperature T. The straight line corresponds to the fit $c_{eq} = e^{-3/T}$. (*B*) Equilibrium height correlations at various temperatures. The main graph shows $\langle [h(r) - h(0)]^2 \rangle$ as a function of distance r. As the defect concentration decreases with decreasing temperature, the curves approach the ideal tiling behavior $\langle [h(r) - h(0)]^2 \rangle = 9/\pi^2 \ln(r)$. (*Inset*) The correlation function $\langle e^{ik\Delta/h(r)} \rangle$, where $\Delta h(r) \equiv h(r) - h(0)$, for $k = \pi/5$; the correlation behaves in a similar way for other choices of k. The dashed line is the power-law behavior for the ideal tiling, $r^{-9k^2/2\pi^2} = r^{-9/50}$ for this choice of k. Once again, the lower the temperature, the longer the algebraic regime. For one of the temperatures, $T = 0.4$, we show that $\langle e^{ik\Delta h(r)} \rangle = e^{-k^2/2\langle [h(r)-h(0)]^2 \rangle}$, as expected from a Gaussian form of the free-energy for the height. (*C*) Scheme for obtaining the height representation of a tiling. A displacement along a tile edge leads to an increase in height by +1 or −1 as shown (cf. Fig. 1).

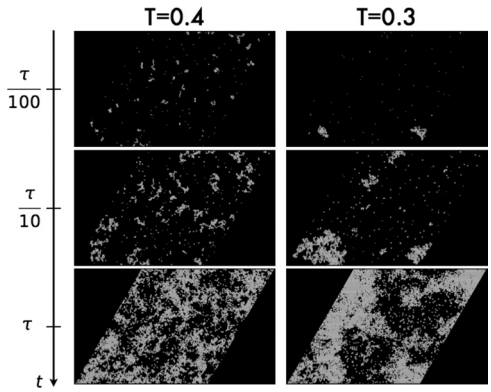

Fig. 4. Dynamic heterogeneity in random rhombus tilings. The images show the persistence field $P_i(t)$ of the local autocorrelation function $C_i(t)$ (see text) at various times t, for representative equilibrium trajectories, at two different temperatures T. Black indicates $P_i(t) = 1$, and white indicates $P_i(t) = 0$. The average relaxation time is τ (see Fig. 5). Relaxation is clearly heterogeneous. The size of dynamic heterogeneity grows with decreasing temperature.

from those of the standard $A + B \rightarrow 0$ problem.[‡] Eventually, for times $t \gg e^{4/T}$, the reverse process $0 \rightarrow A + B$ becomes accessible, and the concentration relaxes to its equilibrium value $c(t) \rightarrow c_{eq}$.[§] The equilibrium properties of the tilings are shown in Fig. 3. The temperature dependence of the equilibrium defect concentration is given by $c_{eq} \approx e^{-3/T}$ (see Fig. 3*A*). This is what one would obtain for a noninteracting gas of defects on the lattice with an energy cost of $E = 3$ per defect. Fig. 3*B* shows the spatial correlations. A rhombus tiling can be mapped to a height field on the triangular lattice (8): The height h changes by ± 1 unit when traversing the edges between tiles, according to the prescription of Fig. 3*C*. The main panel of Fig. 3*B* shows the height–height correlation function, $\langle [h(r) - h(0)]^2 \rangle$, as a function of distance r (along lattice directions), for various temperatures.[¶]

At low temperatures this correlation approaches the ideal tiling limit $\langle [h(r) - h(0)]^2 \rangle = 9/\pi^2 \ln(r)$, corresponding to a Gaussian free-energy $F = \int d^2\vec{x} (K/2) |\partial h(\vec{x})|^2$ for a continuous height field (3), with elastic constant $K = \pi/9$ (8). For finite T the logarithmic behavior is over a finite distance due to the presence of tiling defects (30). An alternative correlation function, $\langle e^{ik[h(r)-h(0)]} \rangle$ (27), is shown in Fig. 3*B Inset*, for the specific value $k = \pi/5$ of the "height space" reciprocal vector (the behavior is similar for other choices of k) (27). At low temperatures the function becomes algebraic indicating long-range correlations. The decay exponent is close to $9k^2/2\pi^2$, as expected from the Gaussian form of the free-energy (27).

As described above, at low temperatures structural rearrangements are most likely in the neighborhood of tiling defects. This gives rise to heterogeneous relaxation, as illustrated in Fig. 4. Here we plot the local autocorrelation function $C_i(t) \equiv \delta_{n_i(t),n_i(0)}$, where n_i stands for the state of site i in the lattice, say $n_i = 0,1,2,3$ for empty, or occupied by a red, green, or blue tile, respectively. More precisely, Fig. 4 shows the corresponding persistence field, $P_i(t) = \Pi_{t'=0}^{t} C_i(t)$: if site i has never relaxed up to time t then $P_i(t) = 1$, and $P_i(t) = 0$ otherwise. The different images show how relaxation is distributed in space at different times. Clearly, the system relaxes in a heterogeneous, spatially correlated manner. Fig. 4 also suggests that the size of these spatial dynamic correlations grows with decreasing temperature. This is very similar to dynamic heterogeneity in structural glass formers (for reviews on dynamic heterogeneity, see refs. 31–34).

Fig. 5 quantifies equilibrium relaxation and dynamic heterogeneity. Fig. 5*A* shows the average (connected and normalized) autocorrelation function $C(t) \equiv (\langle C_i(t) \rangle - A)/(1 - A)$, where $A \equiv \langle C_i(\infty) \rangle = c_{eq}^2 + (1 - c_{eq})^2/3$. As expected, the autocorrelation function decays more slowly the lower the temperature. The characteristic timescale for relaxation, τ, obtained from these correlations is approximately $\tau = \tau_0 e^{\Delta/T}$, with $\tau \approx 6.6$ (see Fig. 5*B*). Relaxation times thus increase with decreasing temperature following an Arrhenius law. In the context of the glass transition, this is often termed "strong" glass-forming behavior (12–14). Moreover, the autocorrelations are close to exponential, rather than stretched exponential (12–14). This could mean that relaxation is not collective, but Fig. 4 suggests otherwise. The exponent Δ appears nontrivial: we have that $\Delta < 7$, the energy barrier to remove two neighboring and parallel tiles (which would allow the adsorption of a distinct tile in the space created); this is the lowest energy barrier to purely local relaxation of the autocorrelation. This indicates that relaxation is achieved more

[‡]We can apply an argument similar to that used in ref. 26 for the XY model. If we think of tiling defects as vortices (27), due to Stokes law, the initial state fluctuations in the difference between upward-pointing and downward-pointing defects in a region of size L scales as $\sqrt{L}$ (26) rather than L (25). If the defects are diffusive, after a time $\Gamma t \sim L^2$, that initial difference is all that will remain, all other defects having annihilated each other (25). The density will then scale as $c(t) \sim \sqrt{L}/L^2 \sim (\Gamma t)^{-3/4}$. (We are grateful to Alan Bray for an important discussion leading to this observation.)

[§]The structural relaxation of random tilings by means of the creation of an opposing pair of defects and their subsequent propagation has been considered before. See for example the "zipper" rearrangements in square–triangle tilings (28).

[¶]An isolated defect in the tiling is a dislocation in the height representation, with Burgers vector of magnitude +3 (−3) for an upward (downward) pointing defect (27). The fluctuations in height can be computed even in the presence of defects by removing the poles in the height field (29). That is, from the height difference $h(\vec{x}) - h(\vec{x}')$ between $\vec{x}$ and $\vec{x}'$, calculated according to the prescription of Fig. 3*C*, the contribution of all defects is subtracted, $h(\vec{x}) - h(\vec{x}') \rightarrow h(\vec{x}) - h(\vec{x}') - \Sigma_k q_k \theta(\vec{x}' - \vec{y}_k, \vec{x} - \vec{y}_k)/2\pi$, where the sum is over all defects k of charge $q_k = \pm 3$ at position $\vec{y}_k$, and $\theta(\vec{a},\vec{b})$ indicates the angle subtended by vectors $\vec{a}$ and $\vec{b}$. This prescription ensures that the corrected height field is single-valued.

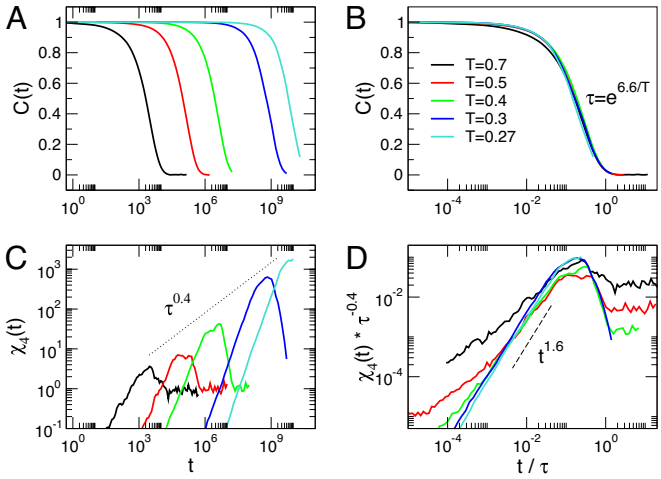

Fig. 5. Relaxation timescales and lengthscales in random rhombus lining. (*A*) Average equilibrium autocorrelation function $C(t)$ at various temperatures T. (*B*) The same as *A* but as a function of scaled time t/τ, showing that the relaxation timescale for the autocorrelation function follows an Arrhenius law, $\tau \propto e^{\Delta/T}$, with $\Delta \approx 6.6$. (*C*) Four-point susceptibility $\chi_4(t)$ at the same temperatures as in *A*. The four-point susceptibility has a maximum at $t \approx \tau$. The peak value appears to scale as $\chi_4^{(peak)} \sim t^{\lambda}$, with $\lambda \approx 0.4$ (see dotted line). (*D*) Scaled susceptibility, $\chi_4(t)/\tau^{\lambda}$ as a function of t/τ. The growth toward the peak would appear to follows the power law $\chi_4 \approx t^{\mu}$, with $\mu \approx 1.6$, at low temperatures.

effectively through defect propagation, a collective mechanism. Interestingly, we also have $\Delta > 6$, which is the value one would expect for diffusing defects, although this may simply be due to logarithmic corrections to diffusion in dimension two.‖

In Fig. 5*C* we show the "four-point" susceptibility, $\chi_4(t) = N(1b - A)^{-2}\ [\langle (1/N^2)\ \Sigma_{ij} C_i(t) C_j(t) \rangle - C^2(t)]$, which measures sample to sample fluctuations in the correlator $C(t)$. This is an observable often used to quantify dynamic heterogeneity (31–37). It measures the degree of spatial fluctuation in the relaxational dynamics, allowing one to uncover spatial dynamical correlations, which are either absent or not apparent in static structural fluctuations. Our observed χ_4 is (*i*) nonmonotonic in time, peaking at times close to the structural relaxation time, $t \approx \tau$, where dynamic heterogeneity is most prominent; and (*ii*) its peak value increases with decreasing temperature, indicating that dynamical fluctuations are larger at lower T. These are two of the central features of χ_4 observed in glass formers (31–34). The four-point susceptibility also displays dynamic scaling at low temperatures, which again seems slightly different from what one expects from diffusing excitations in two dimensions (36): the peak value, $\chi_4^{peak} = \chi_4(\tau)$, appears to scale as a power of the relaxation time, $\chi_{peak}^4 \sim \tau^{\lambda}$, with $\lambda \approx 0.4$ (rather than $\lambda = 1$); and the growth of χ_4 toward the peak goes as $\chi_4(t) \sim t^{\mu}$, with $\mu \approx 1.6$ (rather than $\mu = 2$), see Fig. 5*D*. Better data would be required to confirm these scaling laws.

Discussion

We have shown that random tilings of the kind corresponding to the experimental system of ref. 11 display features commonly associated with glass forming systems, most notably a pronounced slowdown at low temperatures and accompanying heterogeneous relaxational dynamics. In these nearly dynamically arrested tilings, structural relaxation occurs through the propagation of rare localized tiling defects. This is an example of the mechanism of dynamic facilitation (38, 39), whereby defects "facilitate" molecular rearrangements in their immediate vicinity. The fact that defects are scarce at low T and that their motion is activated leads to the observed slowdown, and to fluctuation-dominated, heterogeneous dynamics (39). Relaxation by means of defect propagation-reaction is the hallmark of kinetically constrained models (KCMs) of glasses (40). The dynamics of the random tiling systems studied here is very close to that of these idealized models. For the simple rhombus tiling, when the number of tiles is not conserved, we have found Arrhenius timescales and exponential relaxation. This is similar to the simpler KCMs, such as the Fredrickson–Andersen model (40) in dimensions two or more (41). The observed dynamic scaling properties may suggest, however, that defect dynamics is not simply that of diffusion–annihilation–creation, but this requires further exploration.

It is possible that more complex random tiling systems, such as those giving rise to quasicrystals (3), display even richer slow dynamics, in particular, superArrhenius timescales at low temperatures and stretched relaxation functions.** Random tilings also offer a further testing ground for theories of the glass transition. Specifically, it would be of interest to see whether their slow dynamics can be explained using the "mosaic" perspective on glasses (45, 46). Here we have a system with a finite configurational entropy density given by all of the possible local tiling arrangements, the central tenet of the mosaic approach (45, 46). The mismatch between mosaics, however, does not produce extended interfaces but rather localized defects, which as shown above make the dynamics close to that of KCMs. Can one therefore explain the structural relaxation of these systems via the entropic droplet picture of refs 45 and 46? And could this highlight connections between the mosaic approach and that based on dynamic facilitation and KCMs (47)? Further study will be necessary to address these and other questions.

‖When relaxation is due to propagation of free defects, the persistence function is approximately given by $P(t) \approx e^{-c\mathcal{N}(t)}$, where c is the concentration of defects, and $\mathcal{N}(t)$ is the average number of distinct sites visited by a defect in time t. For diffusing defects in two dimensions, $\mathcal{N}(t) \approx (\Gamma t)/\ln(\Gamma t)$. This, combined with the equilibrium concentration, c_{eq}, gives, up to logarithmic corrections, $P(t) \sim e^{-t/\tau}$, with $\tau \sim c_{eq}^{-1}\ \Gamma^{-1} \propto \exp(6/T)$.

**The relation between quasicrystals and certain glasses has been discussed recently in ref. 42. The slow dynamics of other kind of tilings is studied also in ref. 43. Other random molecular networks with glassy characteristics have been reported in ref. 44.

ACKNOWLEDGMENTS. We thank Chris Henley for correspondence. This work was supported in part by Engineering and Physical Sciences Research Council Grant EP/D048761/1.

1. Fisher ME (1961) Statistical mechanics of dimers on a plane lattice. *Phys Rev* 124:1664–1672
2. Kasteleyn PW (1963) Dimer statistics and phase transitions. *J Math Phys* 4:287–297.
3. Henley CL (1999) in *Quasicrystals, the State of the Art*, eds Di Vincenzo DP, Steinhardt PJ (World Sci, Singapore), pp 459–560.
4. Cohn H, Kenyon R, Propp J (2001) A variational principle for domino tilings. *J Am Math Soc* 14:297–346.
5. Wilson, D B (2004) Mixing times of lozenge tiling and card shuffling Markov chains. *Ann Appl Prob* 14:274–325.
6. Shechtman D, Blech I, Gratias D, Cahn JW (1984) Metallic phase with long-range orientational order and no translational symmetry *Phys Rev Lett* 53:1951–1953.
7. Levine D, Steinhardt PJ (1984) Quasicrystals—A new class of ordered structures. *Phys Rev Lett* 53: 2477–2480.
8. Blote HWJ, Hilborst HJ (1982) Roughening transitions and the zero-temperature triangular ising antiferromagnet. *J Phys A* 15:L631–L637.
9. Moessner R, Sondhi SL, Fradkin E (2002) Short-ranged resonating valence bond physics, quantum dimer models, and ising gauge theories. *Phys Rev B* 65:024504.
10. Castelnovo C, Moessner R, Sondhi SL (2008) Magnetic monopoles in spin ice. *Nature* 451:42–45.
11. Blunt MO, et al. (2008) Random tiling and topological defects in a two-dimensional molecular network. *Science* 322:1077–1081.
12. Ediger MD, Angell CA, Nagel SR (1996) Supercooled liquids and glasses. *J Phys Chem* 100:13200–13212
13. Angell CA, Ngai KL, McKenna GB, McMillan PF, Martin SW (2000) Relaxation in glassforming liquids and amorphous solids. *J Appl Phys* 88:3113–3157

14. Debenedetti PG, Stillinger FH (2001) Supercooled liquids and the glass transition *Nature* 410:259–267.
15. Alet F, et al. (2005) Interacting classical dimers on the square lattice. *Phys Rev Lett* 94:235702.
16. Alet F, et al. (2006) Classical dimers with aligning interactions on the square lattice. *Phys Rev E* 74:041124.
17. Papanikolaou S, Luijten E, Fradkin E (2007) Quantum criticality, lines of fixed points, and phase separation in doped two-dimensional quantum dimer models *Phys Rev B* 76:134514–134528.
18. Jacobsen JL, Alet F (2009) Semiflexible fully packed loop model and interacting rhombus tilings. *Phys Rev Lett* 102:145702.
19. Henley CL (1997) Relaxation time for a dimer covering with height representation. *J Stat Phys* 89:483–507.
20. Bortz AB, Kalos MH, Lebowitz JL (1975) New algorithm for Monte-Carlo simulation of ising spin systems. *J Comp Phys* 17:10–18.
21. Newman MEJ, Barkema GT (1999) *Monte Carlo Methods in Statistical Physics* (Oxford Univ Press, Oxford).
22. Odor G (2004) Universality classes in nonequilibrium lattice systems. *Rev Mod Phys* 76:663–724.
23. Bouttier J, Bowick M, Guitter E, Jeng M (2007) Vacancy localization in the square dimer model. *Phys Rev E* 76:041140.
24. Jeng M, Bowick MJ, Krauth W, Schwarz JM, Xing X (2008) Vacancy diffusion in the triangular-lattice dimer model. *Phys Rev E* 78:021112.
25. Toussaint D, Wilczek F (1983). Particle–antiparticle annihilation in diffusive motion. *J Chem Phys* 78:2642–2647.
26. Mondello M, Goldenfeld N (1990) Scaling and vortex dynamics after the quench of a system with a continuous symmetry. *Phys Rev A* 42:5865–5872.
27. Kondev J, Henley CL (1996) Kac-Moody symmetries of critical ground states. *Nucl Phys B* 464:540–575.
28. Oxborrow M, Henley CL (1993) Random square-triangle tilings: A model for twelve-fold-symmetric quasicrystals. *Phys Rev B* 48:6966–6998.
29. Leung PW, Henley CL, Chester GV (1989) Dodecagonal order in a two-dimensional Lennard-Jones system. *Phys Rev B* 39:446–458.
30. Krauth W, Moessner R (2003) Pocket Monte Carlo algorithm for classical doped dimer models. *Phys Rev B* 67:064503.
31. Sillescu H (2000) Heterogeneity at the glass transition: A review. *J Non-Cryst Solids* 243:81–108
32. Ediger MD (2000) Spatially heterogeneous dynamics in supercooled liquids. *Annu Rev Phys Chem* 51:99–128.
33. Glotzer SC (2000) Spatially heterogeneous dynamics in liquids: Insights from simulation. *J Non-Cryst Solids* 274:342–355.
34. Andersen HC (2005) Molecular dynamics studies of heterogeneous dynamics and dynamic crossover in supercooled atomic liquids. *Proc Natl Acad Sci USA* 102:6686–6691.
35. Glotzer SC, Novikov VN, Schroder TB (2000) Time-dependent, four-point density correlation function description of dynamical heterogeneity and decoupling in supercooled liquids. *J Chem Phys* 112:509–512.
36. Toninelli C, Wyart M, Berthier L, Biroli G, Bouchaud JP (2005) Dynamical susceptibility of glass formers: Contrasting the predictions of theoretical scenarios. *Phys Rev E* 71:041505.
37. Chandler D, Garrahan JP, Jack RL, Maibaum L, Pan AC (2006) Lengthscale dependence of dynamic four-point susceptibilities in glass formers. *Phys Rev E* 74:051501.
38. Fredrickson GH, Andersen HC (1984) Kinetic Ising-model of the glass-transition. *Phys Rev Lett* 53:1244–1247.
39. Garrahan J, Chandler D (2002) Geometrical explanation and scaling of dynamical heterogeneities in glass forming systems. *Phys Rev Lett* 89:035704.
40. Ritort F, Sollich P (2003) Glassy dynamics of kinetically constrained models. *Adv Phys* 52:219–342.
41. Jack RL, Mayer P, Sollich P (2006) Mappings between reaction–diffusion and kinetically constrained systems: $A+A \rightarrow A$ and the Fredrickson–Andersen model have upper critical dimension $d_c = 2$. *J Stat Mech* 2006:P03006.
42. Keys AS, Glotzer SC (2007) How do quasicrystals grow? *Phys Rev Lett* 99:235503.
43. Shokef Y, Lubensky TC (2009) Stripes, zigzags, and slow dynamics in buckled hard spheres. *Phys Rev Lett* 102:048303.
44. Otero R, et al. (2008) Elementary structural motifs in a random network of cytosine adsorbed on a gold(111) surface. *Science* 319:312–315.
45. Xia XY, Wolynes PG (2000) Fragilities of liquids predicted from the random first order transition theory of glasses. *Proc Natl Acad Sci USA* 97:2990–2994.
46. Bouchaud JP, Biroli G (2004). On the Adam-Gibbs-Kirkpatrick-Thirumalai-Wolynes scenario for the viscosity increase in glasses. *J Chem Phys* 121:7347–7354.
47. Jack R, Garrahan J (2005) Caging and mosaic length scales in plaquette spin models of glasses. *J Chem Phys* 123:164508.